Received: 20 January 2023 | Revised: 20 April 2023 | Accepted: 11 July 2023

DOI: 10.1002/bit.28507

ARTICLE

BIOTECHNOLOGY AND BIOENGINEERING WILEY

Continuous polyhydroxybutyrate production from biogas in an innovative two-stage bioreactor configuration

Yadira Rodríguez[1,2] | Silvia García[1,2] | Raquel Lebrero[1,2] | Raúl Muñoz[1,2]

[1]Department of Chemical Engineering and Environmental Technology, School of Industrial Engineering, University of Valladolid, Valladolid, Spain

[2]Institute of Sustainable Processes, Valladolid, Spain

Correspondence
Raúl Muñoz, Department of Chemical Engineering and Environmental Technology, School of Industrial Engineering, University of Valladolid, Dr. Mergelina s/n, Valladolid 47011, Spain.
Email: mutora@iq.uva.es

Funding information
Ministerio de Ciencia e Innovación, Grant/Award Numbers: BES-2016-077160, CTM2015-70442-R; European Regional Development Fund, Grant/Award Numbers: UIC315, CLU2017-09; Junta de Castilla y León, Grant/Award Numbers: UIC315, CLU2017-09

Abstract

Biogas biorefineries have opened up new horizons beyond heat and electricity production in the anaerobic digestion sector. Added-value products such as polyhydroxyalkanoates (PHAs), which are environmentally benign and potential candidates to replace conventional plastics, can be generated from biogas. This work investigated the potential of an innovative two-stage growth-accumulation system for the continuous production of biogas-based polyhydroxybutyrate (PHB) using *Methylocystis hirsuta* CSC1 as cell factory. The system comprised two turbulent bioreactors in series to enhance methane and oxygen mass transfer: a continuous stirred tank reactor (CSTR) and a bubble column bioreactor (BCB) with internal gas recirculation. The CSTR was devoted to methanotrophic growth under nitrogen balanced growth conditions and the BCB targeted PHB production under nitrogen limiting conditions. Two different operational approaches under different nitrogen loading rates and dilution rates were investigated. A balanced nitrogen loading rate along with a dilution rate (D) of 0.3 day^{-1} resulted in the most stable operating conditions and a PHB productivity of ~53 g PHB m^{-3} day^{-1}. However, higher PHB productivities (~127 g PHB m^{-3} day^{-1}) were achieved using nitrogen excess at a D = 0.2 day^{-1}. Overall, the high PHB contents (up to 48% w/w) obtained in the CSTR under theoretically nutrient balanced conditions and the poor process stability challenged the hypothetical advantages conferred by multistage vs single-stage process configurations for long-term PHB production.

KEYWORDS
biogas biorefinery, biopolymers, methane oxidation, methanotrophic bacteria, multi-stage system, polyhydroxyalkanoate production

1 | INTRODUCTION

The production of virgin plastics has risen exponentially since the 1950s, thus intensifying the accumulation of plastic waste in natural environments and landfills (Geyer et al., 2017; UNEP, 2021). Recent studies have highlighted that plastic pollution and climate change, the major global environmental threats nowadays, are intrinsically interconnected. Therefore, both environmental challenges should be addressed jointly: the engagement in finding solutions to plastic problem reinforces actions on climate change mitigation (Ford

et al., 2022). Besides reducing their widespread utilization, substituting conventional plastics by biodegradable bioplastics can significantly contribute to decrease the environmental damage caused by mismanaged plastic waste and to reduce greenhouse gases (GHG) footprint.

Natural polymers such as polyhydroxyalkanoates (PHAs) can be synthetized intracellularly (forming spherical inclusions) by different prokaryotic microorganisms, typically when subjected to nutrient limitation (nitrogen, phosphorous, magnesium, etc.) in the presence of carbon excess (Kourmentza et al., 2017; Urtuvia et al., 2014). PHAs are biocompatible and readily biodegradable in most aerobic (marine, soil, and compost) and anaerobic (landfills, digesters, and sewage sludge) environments (Garcia-Depraect et al., 2021; Meereboer et al., 2020). With similar properties to those of polypropylene (PP), poly(3-hydroxybutyrate) (P3HB) along with its copolymer poly(3-hydroxybutyrate-co-3-hydroxyvalerate (P(3HB-*co*-3HV)) are the most representative of this family of biopolyesters, which encompasses over 150 different monomeric units (Koller et al., 2010; Li et al., 2016; Steinbüchel, 1995). The global production of PHAs accounted for only 1.7% of the bioplastics market in 2020 (2.1 million tonnes [EUBP, 2020]), while the high current PHA demand exceeds supply (Ravenstijn, 2021). Unfortunately, PHAs are not competitively priced in comparison with their petroleum-based counterparts, partly owing to the high costs of the carbon feedstock that dominate process costs (up to 50%) and limits PHA commercialization (e.g. polyhydroxybutyrate [PHB] prices average up to sixfold higher than PP) (Riedel et al., 2015; van den Oever et al., 2017; Vandi et al., 2018).

The need to identify low-cost, nonfood based materials (e.g., wastewater, C1 gases, and lignocellulose or waste vegetable oils) to replace sugars and vegetable oils as a feedstock has triggered an intensive research during the last decade (Jiang et al., 2016; Riedel & Brigham, 2020). Particularly, biogas-based PHB production has emerged as a promising alternative to sugar-based PHB synthesis owing to its high content in methane (50–70%), which can boost the economic sustainability and the environmental benefits of conventional anaerobic digestion (Kapoor et al., 2020; Pieja et al., 2017; Strong et al., 2016). Unlike other renewables energies such as solar photovoltaic or onshore wind, whose levelized electricity costs have declined by 85% and 56% (USD 0.057 and 0.039 kWh^{-1} in 2020) during last decade, respectively, the levelized cost of electricity from biogas has remained constant (USD 0.095–0.19 kWh^{-1}), which requires the development of innovative biogas applications (Fraunhofer, 2021; IRENA, 2021). Furthermore, developing the biogas sector through the exploitation of its vast untapped potential (12065 TWh worldwide) could contribute to the reduction of up to 12% of global GHG emissions (WBA, 2019). In this context, companies such as Mango Materials or Newlight Technologies have emerged to exploit microbial fermentation paths to produce PHAs out of biogas.

The ability to synthetize PHAs out of methane correspond to type-II methane oxidizing bacteria, also known as methanotrophs. These microorganisms aerobically degrade methane (as the sole energy and carbon source) for its assimilation as formaldehyde through the serine pathway (Hanson & Hanson, 1996; Kalyuzhnaya et al., 2019). Within this bacterial group, *Methylocystis hirsuta* CSC1 has been recently pointed out as a workhorse for PHA production (Bordel et al., 2019b; López et al., 2018). The strain was found to grow on biogas and synthetize PHB optimally at 25°C under an O_2:CH_4 atmosphere of 1.6:1 (Chen et al., 2020; Rodríguez et al., 2020b). PHB contents ranging from 43 to 52% have been reported when using biogas and natural gas as carbon substrates, respectively, under batch cultivation (López et al., 2018; Rahnama et al., 2012; Rodríguez, et al., 2020a).

The industrialization of biogas bioconversion into PHA is nowadays challenged by the inherent poor gas-liquid CH_4 mass transfer and the reduced growth rate of methanotrophs under nutrient limiting conditions (Fei, 2015; Jawaharraj et al., 2020). Maximum methane elimination capacities of 91.1 and 74 $g\,m^{-3}\,h^{-1}$ have been achieved in turbulent contactors such as stirred tank and bubble column bioreactors (BCB), respectively (Cantera et al., 2016; Rodríguez et al., 2020b). Unfortunately, limited research devoted to maximize PHAs contents concomitantly with bacterial productivities is available in literature (Blunt et al., 2018; Koller, 2018). The rationale of a multi-stage approach arises from the need of decoupling balanced growth and PHB production, as high growth rates and PHB production rates cannot occur simultaneously (Koller & Muhr, 2014). Previous studies on one-stage systems for PHB production using feast-famine strategies revealed methanotrophic growth on PHB during feast phase, thus reducing the overall PHB yield of the process (Rodríguez et al., 2020b; Rodríguez et al., 2022). Thus, the operation of a two-stage system aims at maximizing both the methanotrophic growth and PHA accumulation, which will ultimately boost PHA productivities and counterbalance the associated higher investment costs. In this context, two-stage processes engineered with a continuous biogas-based cultivation under non nutrient limiting conditions for methanotrophic growth, coupled to a nutrient limited stage devoted to boost PHA accumulation, represents a promising approach that has never been explored in literature.

This work investigated for the first time the potential of a novel two-stage system composed of a continuous stirred tank reactor operated under nitrogen sufficient conditions and a nitrogen-limited BCB engineered with internal gas recirculation to maximize the continuous production of CH_4-based PHB by *M. hirsuta* CSC1. The influence of N loading rate (i.e., excess and balanced N conditions) and dilution rate under balanced nitrogen conditions on process performance was evaluated.

2 | MATERIALS AND METHODS

2.1 | Methanotrophic strain and culture medium

M. hirsuta CSC1 (DSMZ 18500), acquired from Leibniz-Institut DSMZ, was used as a model methanotrophic strain. Subcultures were performed in autoclaved 120-mL serum vials containing 45 mL of mineral salt medium and an O_2:CH_4 headspace (2:1 molar ratio),

inoculated at 10% (v/v), and incubated at 250 rpm and 30°C in a rotary shaker (Thermo Fisher Scientific Inc.) for 7–10 days. The gas headspace was periodically restored upon depletion by flushing filtered O_2 and injecting 25 mL of CH_4 under sterile conditions.

Inoculum preparation and the subsequent experiments were carried out with a mineral salt solution (NMS), unless otherwise stated, containing (mg L^{-1}): KNO_3 (1000); $MgSO_4{\cdot}7H_2O$ (1100); $Na_2HPO_4{\cdot}12H_2O$ (828); KH_2PO_4 (260); $CaCl_2{\cdot}2H_2O$ (200); $CuSO_4{\cdot}5H_2O$ (1); $FeSO_4{\cdot}7H_2O$ (0.5); $ZnSO_4{\cdot}7H_2O$ (0.4); $Na_2MoO_4{\cdot}2H_2O$ (0.4); Fe-EDTA (0.38); $Na_2EDTA{\cdot}2H_2O$ (0.3); $CoCl_2$ (0.03); $MnCl_2{\cdot}4H_2O$ (0.02); H_3BO_3 (0.015) and $NiCl_2{\cdot}6H_2O$ (0.01). The mineral salt medium was adjusted to a pH of 6.8.

2.2 | Chemicals

The aforementioned chemicals and most of the reagents required for PHB analysis (chloroform [≥99%], 1-propanol [99.7%], hydrochloric acid 37% [w/v] and benzoic acid ≥ 99.5%) were purchased from PanReac AppliChem. Poly(3-hydroxybutyrate-co-3-hydroxyvalerate) containing 14% w/w of hydroxyvalerate (HV) was acquired from Sigma-Aldrich. KNO_3 was supplied by COFARCAS (Spain). Synthetic biogas with a CH_4:CO_2 composition of 70:30% (v/v), O_2 (≥99.5%) and CH_4 (≥99.995%) were supplied by Abelló Linde S.A.

2.3 | Experimental set-up

The experiments were conducted in a two-stage system consisting of a stirred tank bioreactor (R1) (Biostat®A, Sartorius Stedim Biotech GmbH) and a BCB (R2) (Plasthermar), with individual working volumes of 2.5 L. R1 was equipped with an automated system for NMS supply and pH, temperature and volume control. Both systems were interconnected via a liquid pump that continuously fed R2 with R1 effluent, maintaining both dilution rates equal. The dilution rate (D), which is expressed as the inflow rate (F) divided by the constant liquid volume (V), was estimated as the maximum specific growth rate (μ_{max}) of *M. hirsuta* during the period of maximum substrate utilization (from Day 5 to 8) under batch cultivation in the stirred tank reactor (R1) (Supporting Information: Figure S1). An additional pump (Watson Marlon 120 S) was periodically activated every 15 min to remove effluent from R2 and maintain a constant volume in R2. An additional pump (Watson Marlon 120 S) was periodically activated (for 15 min every 1 h) to remove effluent from R2 and maintain a constant volume in R2. Liquid level fluctuations in R2 were negligible as they accounted only for 0.83% (20.8 mL) of the total working volume.

A synthetic gas mixture with a ratio O_2:CH_4 (18%:9% v/v) was continuously supplied to both bioreactors at 42 mL min^{-1} via 1 and 3 stainless steel porous spargers (2 µm-pore size, Supelco) in R1 and R2, respectively, and arranged as shown in Figure 1. The gas mixture was obtained by adjusting the flowrate of compressed ambient air and synthetic biogas (70:30% v/v CH_4:CO_2) with a rotameter and a mass flow controller (GFC17, Aalborg^{TM}), respectively. The operating temperature was maintained at 32°C and 25°C in R1 and R2, respectively, whereas the pH was kept at 7.0 with the addition of NaOH (4 N). The Rushton impeller agitation speed in R1 and magnetic agitation in R2 were set at 600 and 500 rpm, respectively. The internal gas recycling in R2 was maintained at 1245 mL min^{-1}.

2.4 | Experimental procedure

2.4.1 | Test 1—nitrogen feeding at a high loading rate

Nitrogen in the form of KNO_3 was provided in excess compared to the N demand in R1, thereby supporting a limited *M. hirsuta* growth in R2 (Table 1). R1 was initially inoculated under strictly sterile conditions at 2% v/v with *M. hirsuta*, resulting in a biomass concentration of 8 mg L^{-1}. After an initial batch phase of 9 days, when the culture was grown in 276 mg N-NO_3^- L^{-1}, autoclaved mineral media with the same N-NO_3^- concentration was fed at a flowrate of 0.5 L day^{-1} in R1, corresponding to a nitrogen loading rate of 56 mg L^{-1} N-NO_3^- day^{-1}. At Day 9, the BCB containing 2 L of nitrogen-free NMS was also interconnected to R1. Both bioreactors were operated at a constant dilution rate of 0.2 day^{-1} for 8 days.

2.4.2 | Test 2—nitrogen feeding at a balanced loading rate

The nitrogen loading matched the nitrogen demand of R1, thus uncoupling completely bacterial growth and PHB synthesis in both bioreactors (Table 1). R1 was initially inoculated under strictly sterile conditions with *M. hirsuta*, resulting in an initial biomass concentration of 22 mg L^{-1}. The continuous operation was carried out in two different stages. After an initial batch phase of 3 days, when the culture was grown in 86 mg N-NO_3–L^{-1}, autoclaved NMS with a N-NO_3^- concentration of 215 mg L^{-1} was fed at a flowrate of 0.5 L day^{-1} in R1, corresponding to a nitrogen loading rate of 44 mg N-NO_3^- L^{-1} day^{-1}. Simultaneously, the BCB containing 2 L of nitrogen-free mineral salt medium was coupled to the system. Both bioreactors were operated at a constant dilution rate of 0.2 day^{-1} for 20 days (Stage I). From Day 23 onwards, the system was operated with a dilution rate of 0.3 day^{-1} and an identical nitrogen loading rate (Stage II).

A daily characterization of the inlet and outlet gas and liquid streams in both bioreactors was performed. The outlet gas flowrate, pressure drop and composition of the inlet and outlet gas streams were measured. Monitoring of the liquid phase (30 mL aliquots) comprised the determination of the pH, optical density (OD) and total suspended solids (TSS) concentration. Duplicate biomass pellets obtained by centrifuging 1.5 mL samples at 10,000 rpm for 10 min were stored at −20°C for PHB analyses. Filtered samples (0.22 µm) were used for the quantification of the total dissolved nitrogen (TN),

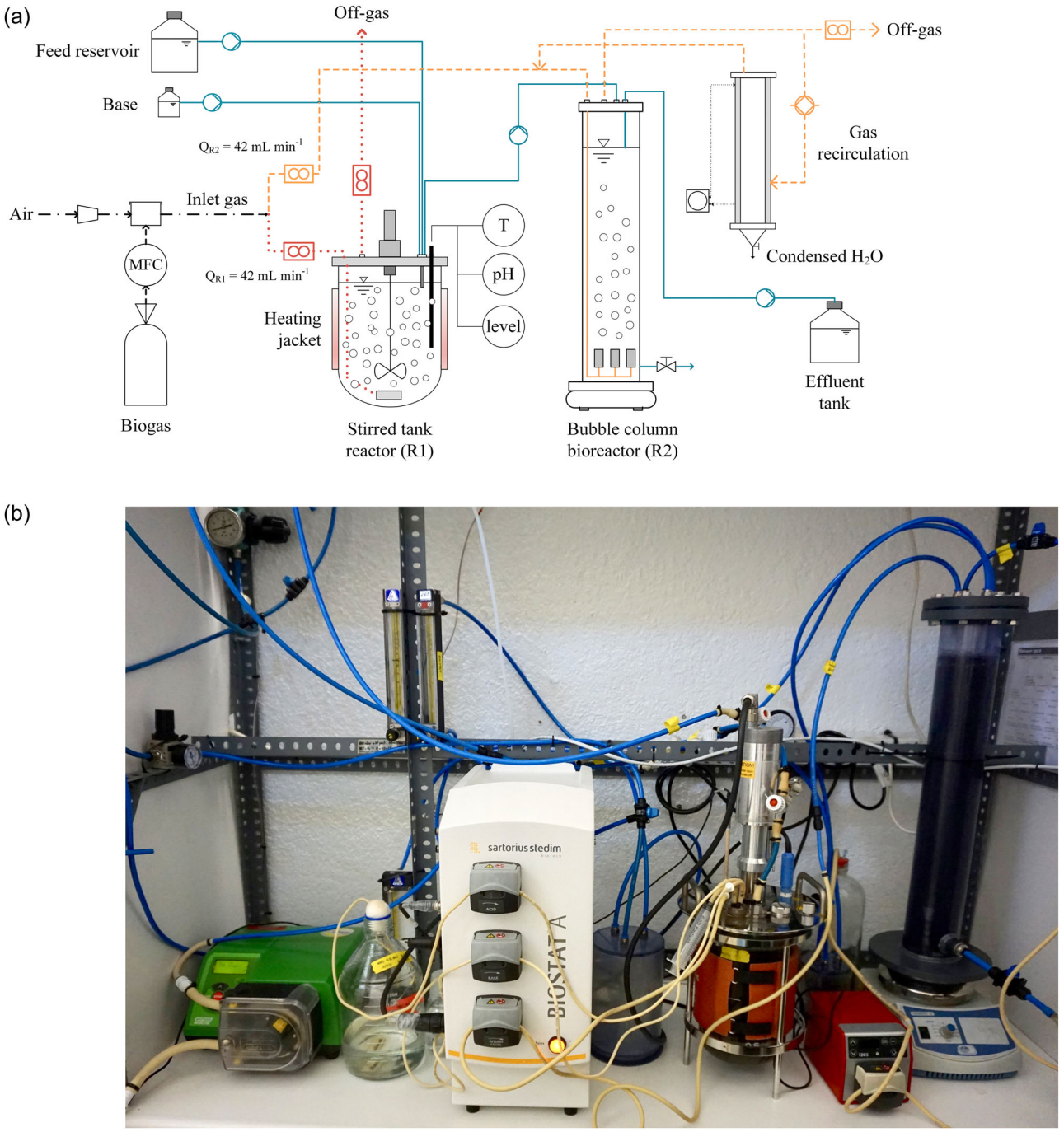

FIGURE 1 (a) Schematic representation and (b) picture of the two-stage bioreactor configuration. Solid line (blue) represents the liquid stream whereas dotted and dashed lines represent gas streams for R1 (red) and R2 (yellow), respectively.

total organic carbon (TOC), and nitrite/nitrate, phosphate and sulphate concentration.

2.5 | Analytical procedures

PHB cell content was determined through gas chromatography-mass spectrometry (GC-MS) using a 7820A GC coupled to a 5977E mass spectrometer (Agilent Technologies). The PHB extraction methodology and GC-MS conditions can be found elsewhere (Chen et al., 2020). Biomass concentration was quantified using Standard Methods (APHA, 2017) as TSSs and culture absorbance using a SPECTROstar Nano at 600 nm (BMG LABTECH). pH measurements were performed using a pH meter Basic 20 (Crison). Ion-exchange liquid chromatography with conductivity detection (Waters 432, Waters Corporation) was used for the determinations of nitrite, nitrate, sulphate and phosphate concentrations. TOC and total nitrogen concentrations were determined in a Shimadzu TOC-$L_{CSH/CSN}$ analyzer equipped with a TNM-1

unit (Shimadzu). Gas flowrates were measured using the water displacement method, whereas CH_4, CO_2, and O_2 concentrations were analyzed in a Bruker 430 gas chromatograph (GC) coupled with a thermal conductivity detector (Bruker Corporation) according to Estrada et al. (2014). An electronic pressure sensor PN7097 (Ifm Electronic) was used to monitor pressure drop.

2.6 | Calculations

The methane elimination capacity (CH_4-EC), methane removal efficiency (CH_4-RE) and volumetric production of CO_2 (PCO_2) were herein used as key performance indicators (KPIs) to assess the performance of both bioreactors:

$$CH_4 - EC = \frac{Q \cdot (C_{CH_4,in} - C_{CH_4,out})}{V_R} \quad (1)$$

$$CH_4 - RE\ (\%) = \frac{C_{CH_4,in} - C_{CH_4,out}}{C_{CH_4,in}} x100 \quad (2)$$

$$PCO_2 = \frac{Q \cdot (C_{CO_2,out} - C_{CO_2,in})}{V_R} \quad (3)$$

where C_{in} and C_{out} are the inlet and outlet CH_4 or CO_2 concentrations (g m^{-3}), respectively, Q is the inlet gas flow ($m^3\ h^{-1}$) and V_R (m^3) is the working volume of the bioreactor.

Based on previously observed performance of the BCB under similar operating conditions, KPI values for CH_4-EC, RE and PCO_2 were 40 g CH_4 m^{-3} h^{-1}, 70% and 80 g CO_2 m^{-3} h^{-1}, respectively.

TABLE 1 Detailed operating conditions for the tests conducted.

Test	Stage	Continuous operation (day)	D (day^{-1})	$N\text{-}NO_3^-$ NMS (mg L^{-1})	$N\text{-}NO_3^-$ Loading Rate (mg $L^{-1}day^{-1}$)	$N\text{-}NO_3^-$ Supply (%)
1	I	8	0.2	276	56	130
2	I	20	0.2	215	44	100
	II	26	0.3	138	44	100

3 | RESULTS AND DISCUSSION

3.1 | Test 1—continuous operation at a high nitrogen loading rate

Following a lag phase period of 2 days, $N\text{-}NO_3^-$ was assimilated in R1 at a rate of 42.4 mg L^{-1} day^{-1} (R = 0.99), being completely depleted by Day 8 (Figure 2a). Total nitrogen concentration

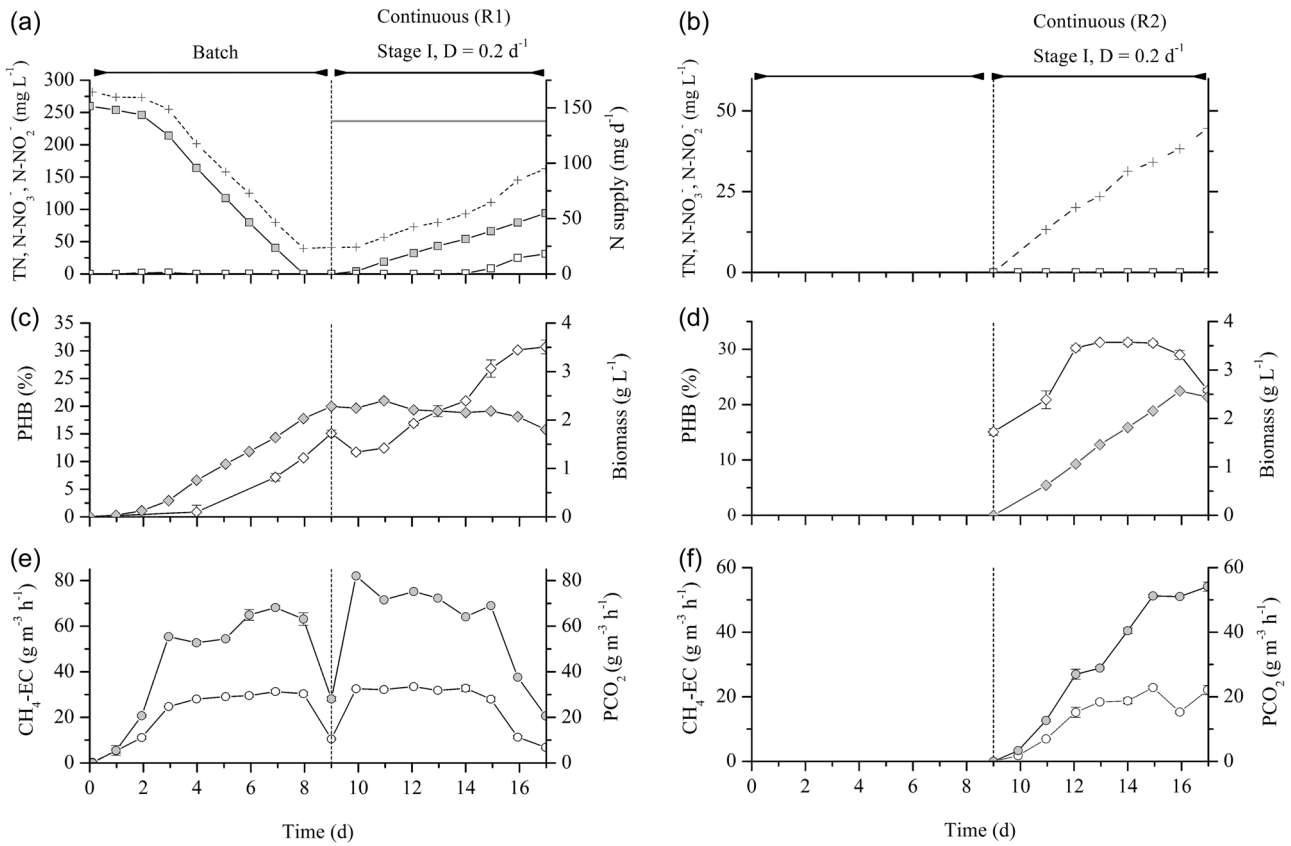

FIGURE 2 Time course of (a, b) total nitrogen (crosses), $N\text{-}NO_3^-$ (solid squares) and $N\text{-}NO_2^-$ (empty squares) concentrations, and N supply (continuous line); (C, D) PHB content (empty diamonds) and biomass concentration (solid diamonds), and (e, f) CH_4-EC (empty circles) and PCO_2 (solid circles) in R1 (left) and R2 (right) during Test 1. Vertical dotted lines separate the different operational stages. PHB, polyhydroxybutyrate.

followed a similar consumption pattern, although a residual TN concentration of ≈40 mg L^{-1} was recorded in the culture broth of R1. The presence of N-NO_2^- during batch cultivation was negligible. The continuous supply of NMS in R1 during stage I resulted in the accumulation of nitrate at a rate of 12.1 mg N-NO_3^- L^{-1} day^{-1} ($R = 0.99$) from Day 10 onwards. A gradual accumulation of N-NO_2^- was also observed in R1 by Day 14 (at concentrations > 54 mg N-NO_3^- L^{-1}), reaching a final concentration of 31.1 mg of N-NO_2^- L^{-1} by Day 17 (Figure 2a). These exposure levels negatively impacted on the methanotrophic fermentation kinetics, as explained further below. In contrast to closely related species (e.g., *Methylocystis* sp. SC2), *M. hirsuta* CSC1 exhibits a truncated denitrification pathway (Bordel et al., 2019a). On the other hand, the residual organic nitrogen concentration was 38.2 ± 1.8 mg L^{-1} during Stage I in R1. In the BCB (R2), neither nitrate nor nitrite concentration was recorded during Test 1 as a result of an active consumption (Figure 2b). A noticeable accumulation of residual organic nitrogen occurred in R2, likely attributed to the organic nitrogen-rich effluent from R1.

Cultivation under batch conditions in R1 resulted in a biomass concentration of 2.3 g TSS L^{-1} by Day 9, and a biomass productivity of 0.32 g L^{-1} day^{-1}. In this context, the maximum specific growth rate of *M. hirsuta* was 0.21 day^{-1} ($R = 0.998$) from Day 5 to 8. The biomass concentration remained constant from Day 9 to 15 (Stage I), averaging 2.2 ± 0.1 g L^{-1}. However, a decrease in biomass productivity was observed during the last 2 days of operation, when biomass concentration dropped to 1.8 ± 0.0 g TSS L^{-1} (Figure 2c). Interestingly, synthesis of PHB was observed during the batch cultivation period in spite of the non-nitrogen limiting conditions. Indeed, PHB synthesis was initiated 3–4 days after inoculation, reaching a final content of 15.1 ± 0.6% at the end of the batch period. It can be hypothesized that the culture experienced growth limiting conditions from Day 3 to 4, generated by factors others than nitrogen availability (i.e., high temperature and high shear stress). The influence of environmental parameters such as temperature, O_2 to CH_4 ratio, and nitrogen source on *M. hirsuta* growth and PHA synthesis has been assessed previously by Rodríguez et al. (2020b). On the other hand, the stirring velocity had been optimized in the same bioreactor (R1) using a methanotrophic mixed culture and same temperature conditions (not published data), leading to optimal removal efficiencies at 600 rpm. Then, elucidating the optimal stirring velocity for this particular strain and evaluating temperature fluctuations (±3°C) occurring in R1 during operation would need to be further addressed to rule out other possible limiting factors.

Process operation under continuous mode entailed a slight decrease in PHB content during the first 24 h. However, from Day 10 onwards PHB cell content steadily increased up to 30.7% by Day 17 despite nitrogen availability in R1. These results agreed with the observations of Rahnama et al. (2012), who claimed that PHB is a growth associated metabolite in *M. hirsuta*, unlike in other type II methanotrophs. These authors observed an increasing PHB production concomitant with an increasing growth rate using a modified NMS. These observations differ markedly with the majority of studies on PHB synthesis by *M. hirsuta*, in which growth-associated PHB production did not occur (López et al., 2018; Rodríguez et al., 2020a). These discrepancies highlight the complexity of the regulatory mechanisms underlying PHB production in methanotrophs and evidence the need for further research. On the other hand, R2 exhibited higher values of biomass concentration (2.6 ± 0.0 g L^{-1} by Day 16) than R1, likely due to the complete utilization of the nitrogen received from R1 (Figure 2d). Similarly, higher PHB values were observed in R2 during continuous operation. Thus, PHB cell content increased from 15.1 ± 0.6% (Day 9) to 30.2 ± 0.5% (Day 12), remaining constant afterwards (30.6 ± 0.1%), which entailed a PHB productivity of 126.7 ± 18.2 g PHB m^{-3} day^{-1} (Figure 2d). The productivity herein recorded was two to threefold higher than the values obtained in a single-stage BCB under N feast-famine cycles (40–60 g PHB m^{-3} day^{-1}) using *M. hirsuta* (Rodríguez et al., 2020b). Unfortunately, the system did not support a stable PHB productivity since PHB content decreased to 22.6 ± 1.0% by Day 16. This drop in the PHB content was likely due to the accumulation of nitrate occurring in R1, which originated a nitrogen-rich effluent and an associated increased N loading rate in R2. These values were nearly the same that the estimated N demand of R2 (20.6 mg N L^{-1} day^{-1}) for the corresponding EC 19.5 g m^{-3} h^{-1}, favouring balance growth conditions and PHB consumption.

R1 initially exhibited a rapid increase in CH_4-EC, overcoming biological limitation by Day 3 and reaching a stable value of 29.6 ± 1.2 g m^{-3} h^{-1} from Day 3 to 8 of batch operation, which corresponded to a removal efficiency of 54.8 ± 3.3% (Figure 2e). Similarly, PCO_2 averaged 59.8 ± 6.4 g m^{-3} h^{-1} in the aforementioned period. By Day 9, both CH_4-EC and PCO_2 values dropped sharply to 10.5 g CH_4 m^{-3} h^{-1} and 28.1 g CO_2 m^{-3} h^{-1}, respectively, as a result of the lack of assimilable nitrogen (i.e., N-NO_3^-) in the culture broth. At this point, the mineralization ratio (PCO_2/EC) increased from 2.0 ± 0.2 (Days 3–8) to 2.7 g CO_2 g^{-1} CH_4, corresponding to an increase in the mineralization from 74 ± 6% to 97%. Both CH_4-EC and PCO_2 were restored following the continuous supply of NMS, achieving values of 32.5 ± 0.6 g CH_4 m^{-3} h^{-1} and 72.4 ± 6.0 g CO_2 m^{-3} h^{-1}, respectively, from Day 10 to 15. Surprisingly, from Day 15 onwards, process performance decreased by nearly 5 times in R1 (Figure 2e), supporting a CH_4-EC of 6.8 g CH_4 m^{-3} h^{-1}, which corresponded to a removal efficiency of 11.4%, by the end of Test 1. It might be inferred that a partial nitrate denitrification to nitrite prevailed over assimilatory pathways when PHB contents are high (>25%) in presence of nitrogen excess, causing a severe nonreversible inhibition of the methanotrophic metabolism due to nitrite. Nitrite, like other small metal ligands such as azide or cyanide, is regarded as an inhibitor of the formate dehydrogenase (FDH) activity. The reaction catalyzed by FDH generates NADH, which is required by the methane monoxygenase to initiate the methane conversion into methanol (Jollie & Lipscomb, 1990).

In R2, CH_4-EC of 19.5 ± 3.1 g CH_4 m^{-3} h^{-1} were achieved from Day 12 onwards, while PCO_2 increased steadily up to 52.1 ± 1.7 g CO_2 m^{-3} h^{-1} by the end of Test 1.

3.2 | Test 2—continuous operation at a balanced nitrogen loading rate

Approximately 46% of the initial nitrate concentration was consumed during batch cultivation, reaching a final concentration of 49.5 mg L^{-1} $N\text{-}NO_3^-$ with no nitrite accumulation observed by Day 3 (Figure 3a). Unlike Test 1, the total nitrogen present in the culture broth corresponded solely to nitrogen in the form of nitrate. Nitrate remained constant at 48.8 ± 0.9 mg $N\text{-}NO_3^-$ L^{-1} from Day 3 to 7 in R1 during process operation at D = 0.2 day^{-1} (Figure 3a). Subsequently, a decrease in nitrate concentration to 18.1 mg L^{-1} occurred from Day 7 to 12, followed by a period of accumulation where $N\text{-}NO_3^-$ increased up to 76.0 mg L^{-1}. These fluctuations in nitrogen consumption might be related to shifts in the N demand during PHB synthesis/consumption (see Figure 3c). The increase in the dilution rate to 0.3 day^{-1} resulted in a stabilization of the $N\text{-}NO_3^-$ concentration at 72.6 ± 3.0 mg L^{-1}, except from Days 35 to 45 when it fluctuated between ≈31 and 73 mg L^{-1} (Figure 3a). The decrease observed in the aforementioned period was probably due to a higher methanotrophic activity mediated by PHB consumption. Only minor peaks of nitrite (<3.6 mg L^{-1} $N\text{-}NO_2^-$) were recorded, whereas the residual organic nitrogen ranged from 9 to 23 mg L^{-1} during Test 2. On the other hand, nitrate concentration in R2 remained below 6 mg L^{-1} $N\text{-}NO_3^-$ from Day 3 to 19, which indicated an almost complete assimilation (Figure 3b). Conversely, an increase in $N\text{-}NO_3^-$ concentration was observed by Day 20 (Stage I) induced by the deterioration in the system performance and the concomitant nitrate accumulation in R1 (Figure 3a,e). Nitrate concentration in R2 increased until Day 28 of operation (Stage II) achieving a maximum value of 44.0 mg L^{-1}. From Day 28 onwards, R2 exhibited again a complete removal of nitrate. No significant accumulation of nitrite occurred along this test in R2 (<3.5 mg L^{-1} $N\text{-}NO_2^-$) (Figure 3b). At the end of Stage I, the residual organic nitrogen concentration in R2 achieved a maximum value of ≈45 mg L^{-1}, while process operation at 0.3 day^{-1} maintained the residual organic nitrogen at 11 mg L^{-1} by the end of Stage II (Figure 3b).

Biomass concentration increased from 0.02 ± 0.00 to 0.37 ± 0.01 g TSS L^{-1} by Day 3 in R1, and continued increasing during continuous operation at D = 0.2 day^{-1} up to a concentration of 1.69 ± 0.00 g L^{-1} (Figure 3c). The increase in the dilution rate, along with the deterioration in methane biodegradation performance, resulted in a steady decrease of biomass concentration from Day 23 to 30, stabilizing from Day 31 onwards at 0.79 ± 0.13 g L^{-1} in R1. Synthesis of PHB was rapidly initiated after inoculation, a PHB content of 25.9% being recorded by Day 3 despite nitrogen availability (Figure 3c). During Stage I, PHB content increased up to

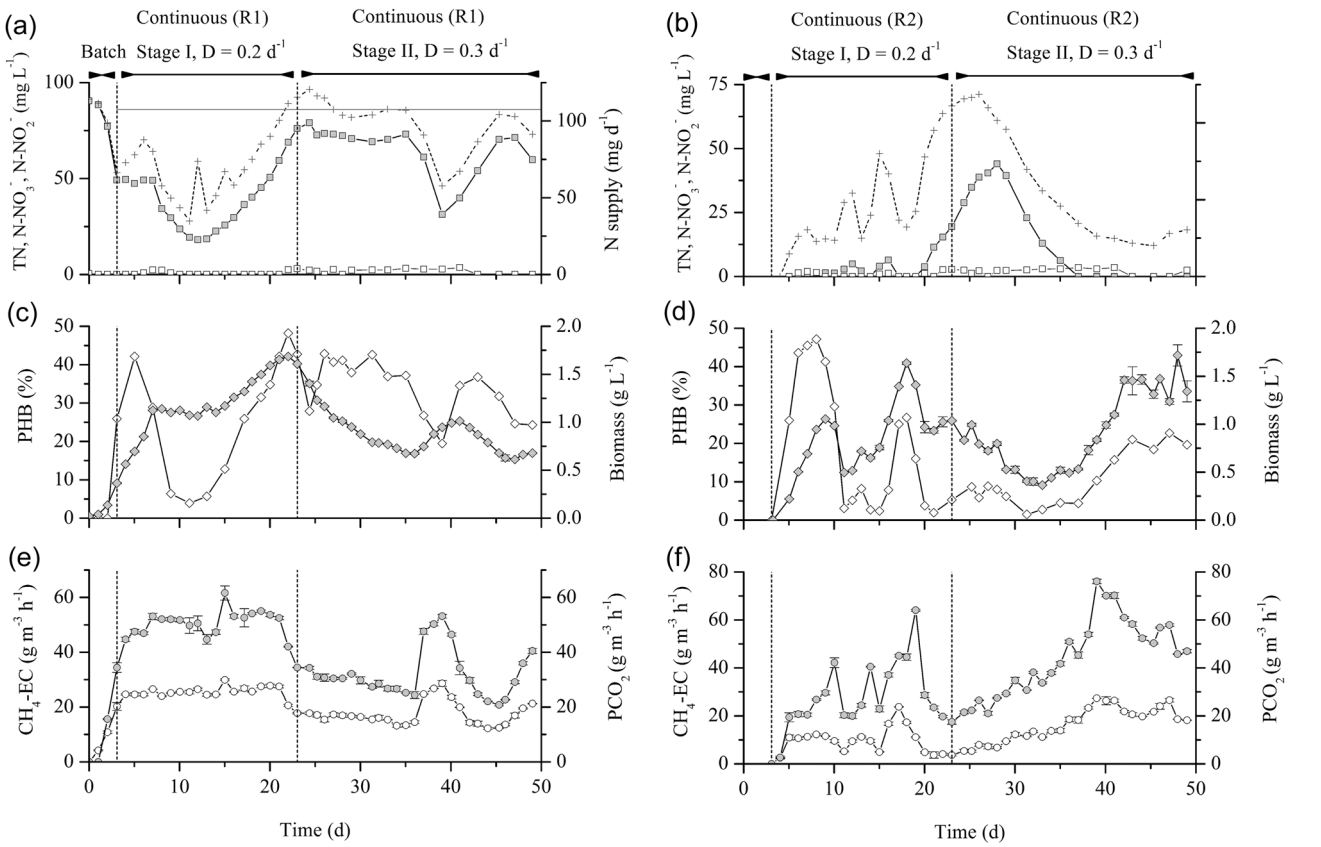

FIGURE 3 Time course of (a, b) total nitrogen (crosses), $N\text{-}NO_3^-$ (solid squares) and $N\text{-}NO_2^-$ (empty squares) concentrations, and N supply (continuous line); (c, d) PHB content (empty diamonds) and biomass concentration (solid diamonds), and (e, f) CH_4-EC (empty circles) and PCO_2 (solid circles) in R1 (left) and R2 (right) during Test 2. Vertical dotted lines separate the different operational stages.

42.1% by Day 5, but rapidly declined to 3.9% w/w by Day 11. Interestingly, PHB synthesis was resumed again, reaching a maximum PHB content of 48.2% by Day 22 likely due to the low nitrogen concentrations (18.1 mg $N\text{-}NO_3^-$ L^{-1}). Process operation at D = 0.3 day^{-1} resulted in a slight decrease in PHB content followed by a stabilization at 33.4 ± 7.8% during the rest of the experiment. On the other hand, biomass concentrations in R2 remained below those values recorded in R1 during Stage I, suggesting biomass decay especially from Day 11 to 15 when the culture was subjected to more severe nitrate limiting conditions in R2 (Figure 3d). After a steady decrease at the beginning of Stage II caused by the higher dilution rate, biomass concentration increased and stabilized at values of 1.43 ± 0.14 g L^{-1}. PHB contents in R2 during Stage I followed a similar trend to the one observed in R1, although superior PHB contents were only recorded by Day 8 (47.1%). In this period, PHB productivities ranged from 3.5 to 89.1 g PHB m^{-3} day^{-1}. PHB contents during process operation at D = 0.3 day^{-1} remained low until Day 37 (5.6 ± 2.4%) and increased from Day 37 to 43 up to 20.5 ± 1.8%, which corresponded to PHB productivities of 53.2 ± 4.8 g PHB m^{-3} day^{-1}. PHB productivities ranging from 40 to 60 g PHB m^{-3} day^{-1} were achieved by *M. hirsuta* in a BCB subjected to 24 h:24 h feast-famine cycles and similar working volume (Rodríguez et al., 2020b).

The methane elimination capacity and volumetric CO_2 production in R1 steeply increased to 20.2 ± 1.4 g CH_4 m^{-3} h^{-1} and 34.4 ± 1.8 g CO_2 m^{-3} h^{-1}, respectively, during batch cultivation (Figure 3e). Both parameters remained stable during Stage I, averaging 25.9 ± 1.5 g CH_4 m^{-3} h^{-1} (corresponding to a RE of 44.3 ± 1.8%) and 51.3 ± 4.1 g CO_2 m^{-3} h^{-1} for CH_4-EC and PCO_2, respectively. These figures are in agreement with the elimination capacities recorded by close relative species such as *Methylocystis parvus* (Rodríguez et al., 2022) and a methanotrophic consortium (Rocha-Rios et al., 2010) in a stirred tank reactor at similar stirring velocities. From Day 21 to 23, a deterioration of the biodegradation performance of R1 was observed, which resulted in CH_4-EC and PCO_2 of 17.8 ± 0.3 and 34.4 ± 0.1 g m^{-3} h^{-1}, respectively. Nonetheless, the mineralization ratio (PCO_2/EC) remained constant at 2.0 ± 0.1 g CO_2 g^{-1} CH_4 (corresponding to a 72 ± 3% mineralization) throughout Stage I. This decrease in biodegradation performance corresponded to the period that exhibited both the highest PHB accumulation (48% w/w) and highest accumulation of TOC (≈124 mg L^{-1}). Further investigations are required to rule out the possibility of inhibition caused by carbon intermediates such as formaldehyde, which is regarded as the most toxic among aldehydes for methylotrophs (Marx et al., 2004). The increase in the dilution rate to 0.3 day^{-1} entailed steady state CH_4-EC and PCO_2 of 15.8 ± 1.4 g m^{-3} h^{-1} and 29.1 ± 2.9 g m^{-3} h^{-1}, corresponding to a PCO_2/EC of 1.8 ± 0.1 g CO_2 g^{-1} CH_4 (67 ± 4% mineralization). This stable process operation may be attributed to the further reduction of TOC concentration (down to ≈60 mg L^{-1}) caused by the higher mineral medium renewal. Interestingly, CH_4-EC increased up to 28.6 ± 1.1 g m^{-3} h^{-1} by Day 39 concomitantly with PHB utilization and an increase in biomass growth (Figure 3e). On the other hand, CH_4-EC and PCO_2 in R2 fluctuated according to the biomass concentration. Thus, CH_4-EC averaged 11.1 ± 0.9 g CH_4 m^{-3} h^{-1} from Days 5 to 10, corresponding to a RE of 42.4% and a PCO_2 of 42.2 ± 2.0 g CO_2 m^{-3} h^{-1} (Figure 3f). Afterwards, PCO_2 and CH_4-EC fluctuated from 20 to 64 g CO_2 m^{-3} h^{-1} and from 4 to 24 g CH_4 m^{-3} h^{-1}, respectively, during Stage I. Process operation at a dilution rate of 0.3 day^{-1} stabilized CH_4-EC and PCO_2 at 22.9 ± 3.3 g CH_4 m^{-3} h^{-1} and 58.3 ± 9.6 g CO_2 m^{-3} h^{-1}, respectively, by the end of Stage II (Figure 3f). Microscopic images of the culture in this period (Supporting Information: Figure S2) revealed the presence of protozoa in R2, which could explain the low values of CH_4-EC recorded in spite of the high biomass concentration.

4 | CONCLUSIONS

This work constitutes the first attempt to continuously produce PHB from biogas using a two-stage growth-accumulation strategy. Continuous cultivation of *M. hirsuta* in the stirred tank reactor at 600 rpm and 32°C likely mediated a physiological stress that induced PHB synthesis under nitrogen availability with intracellular PHB contents of 48% w/w. The increase in the dilution rate from 0.2 to 0.3 day^{-1} allowed for a process stabilization at the expenses of a reduced methane elimination capacity (~16 g CH_4 m^{-3} h^{-1}) and overall PHB productivities in the system of ~53 g PHB m^{-3} day^{-1}. Under the conditions applied, the second bioreactor did not support significantly enhanced PHB accumulations. Further investigations are required to improve process robustness under continuous operation in this innovative two-stage configuration.

AUTHOR CONTRIBUTIONS

Yadira Rodríguez: Conceptualization, methodology, investigation, formal analysis, visualization, writing—original draft. **Silvia García**: Investigation. **Raquel Lebrero**: Conceptualization, funding acquisition, supervision, writing—review and editing. **Raúl Muñoz**: Conceptualization, funding acquisition, supervision, writing—review and editing.

ACKNOWLEDGMENTS

This research was funded by the Spanish Ministry of Science and Innovation under BES-2016-077160 contract and CTM2015-70442-R project. The support from the EU-FEDER program and the regional government of Castilla y León (UIC 315, CLU 2017-09) is acknowledged. Authors would like to thank J. Prieto and E. Marcos for their practical support during PHA extraction and GC-MS analyses, respectively.

CONFLICT OF INTEREST STATEMENT

The authors declare no conflict of interest.

DATA AVAILABILITY STATEMENT

Research data are not shared.

ORCID

Yadira Rodríguez http://orcid.org/0000-0003-1979-8254
Silvia García https://orcid.org/0000-0003-2083-833X
Raquel Lebrero https://orcid.org/0000-0002-3033-8649
Raúl Muñoz http://orcid.org/0000-0003-1207-6275

REFERENCES

APHA. (2017). *Standard methods for the examination of water and wastewater*. 23rd ed., American Public Health Association.

Blunt, W., Levin, D., & Cicek, N. (2018). Bioreactor operating strategies for improved polyhydroxyalkanoate (PHA) productivity. *Polymers*, *10*, 1197.

Bordel, S., Rodríguez, E., & Muñoz, R. (2019a). Genome sequence of *Methylocystis hirsuta* CSC1, a polyhydroxyalkanoate producing methanotroph. *MicrobiologyOpen*, *8*, e00771.

Bordel, S., Rodriguez, Y., Hakobyan, A., Rodriguez, E., Lebrero, R., & Munoz, R. (2019b). Genome scale metabolic modeling reveals the metabolic potential of three Type II methanotrophs of the genus Methylocystis. *Metabolic Engineering*, *54*, 191–199.

Cantera, S., Estrada, J. M., Lebrero, R., García-Encina, P. A., & Muñoz, R. (2016). Comparative performance evaluation of conventional and two-phase hydrophobic stirred tank reactors for methane abatement: Mass transfer and biological considerations. *Biotechnology and Bioengineering*, *113*, 1203–1212.

Chen, X., Rodríguez, Y., López, J. C., Muñoz, R., Ni, B.-J., & Sin, G. (2020). Modeling of polyhydroxyalkanoate synthesis from biogas by *Methylocystis hirsuta*. *ACS Sustainable Chemistry & Engineering*, *8*, 3906–3912.

Estrada, J. M., Lebrero, R., Quijano, G., Pérez, R., Figueroa-González, I., García-Encina, P. A., & Muñoz, R. (2014). Methane abatement in a gas-recycling biotrickling filter: Evaluating innovative operational strategies to overcome mass transfer limitations. *Chemical Engineering Journal*, *253*, 385–393.

EUBP. (2020). *Bioplastics market data. European Bioplastics*.

Fei, Q. (2015). Benefits and hurdles for biological methane upgrading, *Sustainable chemicals & plastics adoptions & applications summit* (pp. 1–12).

Ford, H. V., Jones, N. H., Davies, A. J., Godley, B. J., Jambeck, J. R., Napper, I. E., Suckling, C. C., Williams, G. J., Woodall, L. C., & Koldewey, H. J. (2022). The fundamental links between climate change and marine plastic pollution. *Science of the Total Environment*, *806*, 150392.

Fraunhofer. (2021). *Levelized cost of electricity renewable energy technologies. FRAUNHOFER Institute for Solar Energy Systems ISE*.

Garcia-Depraect, O., Bordel, S., Lebrero, R., Santos-Beneit, F., Börner, R. A., Börner, T., & Muñoz, R. (2021). Inspired by nature: Microbial production, degradation and valorization of biodegradable bioplastics for life-cycle-engineered products. *Biotechnology Advances*, *53*, 107772.

Geyer, R., Jambeck, J. R., & Law, K. L. (2017). Production, use, and fate of all plastics ever made. *Science Advances*, *3*, e1700782.

Hanson, R. S., & Hanson, T. E. (1996). Methanotrophic bacteria. *Microbiological Reviews*, *60*, 439–471.

IRENA. (2021). *Renewable power generation costs in 2020. International Renewable Energy Agency*.

Jawaharraj, K., Shrestha, N., Chilkoor, G., Dhiman, S. S., Islam, J., & Gadhamshetty, V. (2020). Valorization of methane from environmental engineering applications: A critical review. *Water Research*, *187*, 116400.

Jiang, G., Hill, D., Kowalczuk, M., Johnston, B., Adamus, G., Irorere, V., & Radecka, I. (2016). Carbon sources for polyhydroxyalkanoates and an integrated biorefinery. *International Journal of Molecular Sciences*, *17*, 1157.

Jollie, D. R., & Lipscomb, J. D. (1990). Formate dehydrogenase from *Methylosinus trichosporium* OB3b. *Methods in Enzymology*, *188*, 331–334.

Kalyuzhnaya, M. G., Gomez, O. A., & Murrell, J. C. (2019). The Methane-Oxidizing Bacteria (Methanotrophs). In: T. J. McGenity (ed.), *Taxonomy, Genomics and Ecophysiology of Hydrocarbon-Degrading Microbes* (pp. 1–34). Springer International Publishing.

Kapoor, R., Ghosh, P., Tyagi, B., Vijay, V. K., Vijay, V., Thakur, I. S., Kamyab, H., Nguyen, D. D., & Kumar, A. (2020). Advances in biogas valorization and utilization systems: A comprehensive review. *Journal of Cleaner Production*, *273*, 123052.

Koller, M. (2018). A review on established and emerging fermentation schemes for microbial production of polyhydroxyalkanoate (PHA) biopolyesters. *Fermentation*, *4*, 30.

Koller, M., Atlić, A., Dias, M., Reiterer, A., & Braunegg, G. (2010). Microbial PHA Production from Waste Raw Materials. In: G. G.-Q. Chen, (ed.), *Plastics from Bacteria: Natural Functions and Applications* (pp. 85–119). Springer Berlin Heidelberg.

Koller, M., & Muhr, A. (2014). Continuous production mode as a viable Process-Engineering tool for efficient Poly(hydroxyalkanoate) (PHA) Bio-Production. *Chemical and Biochemical Engineering Quarterly*, *28*(1), 65–77.

Kourmentza, C., Plácido, J., Venetsaneas, N., Burniol-Figols, A., Varrone, C., Gavala, H. N., & Reis, M. A. M. (2017). Recent advances and challenges towards sustainable polyhydroxyalkanoate (PHA) production. *Bioengineering*, *4*, 55.

Li, Z., Yang, J., & Loh, X. J. (2016). Polyhydroxyalkanoates: Opening doors for a sustainable future. *NPG Asia Materials*, *8*, e265.

López, J. C., Arnáiz, E., Merchán, L., Lebrero, R., & Muñoz, R. (2018). Biogas-based polyhydroxyalkanoates production by *Methylocystis hirsuta*: A step further in anaerobic digestion biorefineries. *Chemical Engineering Journal*, *333*, 529–536.

Marx, C. J., Miller, J. A., Chistoserdova, L., & Lidstrom, M. E. (2004). Multiple formaldehyde oxidation/detoxification pathways in *Burkholderia fungorum* LB400. *Journal of Bacteriology*, *186*, 2173–2178.

Meereboer, K. W., Misra, M., & Mohanty, A. K. (2020). Review of recent advances in the biodegradability of polyhydroxyalkanoate (PHA) bioplastics and their composites. *Green Chemistry*, *22*, 5519–5558.

van den Oever, M., Molenveld, K., van der Zee, M., & Bos, H. (2017). *Bio-based and biodegradable plastics - Facts and Figures*. Wageningen UR.

Pieja, A. J., Morse, M. C., & Cal, A. J. (2017). Methane to bioproducts: The future of the bioeconomy? *Current Opinion in Chemical Biology*, *41*, 123–131.

Rahnama, F., Vasheghani-Farahani, E., Yazdian, F., & Shojaosadati, S. A. (2012). PHB production by *Methylocystis hirsuta* from natural gas in a bubble column and a vertical loop bioreactor. *Biochemical Engineering Journal*, *65*, 51–56.

Ravenstijn, J. (2021). *Fast growing PHA demand and new capacities, but what about legislation?* (pp. 1–33).

Riedel, S. L., & Brigham, C. J. (2020). Inexpensive and Waste Raw Materials for PHA production. In M. Koller (Ed.), *The Handbook of Polyhydroxyalkanoates: Microbial Biosynthesis and Feedstocks* (1st ed). CRC Press.

Riedel, S. L., Jahns, S., Koenig, S., Bock, M. C. E., Brigham, C. J., Bader, J., & Stahl, U. (2015). Polyhydroxyalkanoates production with *Ralstonia eutropha* from low quality waste animal fats. *Journal of Biotechnology*, *214*, 119–127.

Rocha-Rios, J., Muñoz, R., & Revah, S. (2010). Effect of silicone oil fraction and stirring rate on methane degradation in a stirred tank reactor. *Journal of Chemical Technology & Biotechnology*, *85*(3), 314–319.

Rodríguez, Y., Firmino, P. I. M., Arnaiz, E., Lebrero, R., & Munoz, R. (2020a). Elucidating the influence of environmental factors on biogas-based polyhydroxybutyrate production by *Methylocystis hirsuta* CSC1. *The Science of the Total Environment*, *706*, 135136.

Rodríguez, Y., Firmino, P. I. M., Pérez, V., Lebrero, R., & Muñoz, R. (2020b). Biogas valorization via continuous polyhydroxybutyrate production by *Methylocystis hirsuta* in a bubble column bioreactor. *Waste Management*, *113*, 395–403.

Rodríguez, Y., García, S., Pérez, R., Lebrero, R., & Muñoz, R. (2022). Optimization of nitrogen feeding strategies for improving polyhydroxybutyrate production from biogas by *Methylocystis parvus* str. OBBP in a stirred tank reactor. *Chemosphere*, *299*, 134443.

Steinbüchel, A. (1995). Diversity of bacterial polyhydroxyalkanoic acids. *FEMS Microbiology Letters*, *128*, 219–228.

Strong, P., Laycock, B., Mahamud, S., Jensen, P., Lant, P., Tyson, G., & Pratt, S. (2016). The opportunity for High-Performance biomaterials from methane. *Microorganisms*, *4*, 11.

UNEP. (2021). *Drowning in plastics—Marine litter and plastic waste vital graphs. United Nations Environment Programme (UNEP).*

Urtuvia, V., Villegas, P., González, M., & Seeger, M. (2014). Bacterial production of the biodegradable plastics polyhydroxyalkanoates. *International Journal of Biological Macromolecules*, *70*, 208–213.

Vandi, L.-J., Chan, C., Werker, A., Richardson, D., Laycock, B., & Pratt, S. (2018). Wood-PHA composites: Mapping opportunities. *Polymers*, *10*, 751.

WBA. (2019). *Global potential of biogas. World Biogas Association*.

SUPPORTING INFORMATION

Additional supporting information can be found online in the Supporting Information section at the end of this article.

How to cite this article: Rodríguez, Y., García, S., Lebrero, R., & Muñoz, R. (2023). Continuous polyhydroxybutyrate production from biogas in an innovative two-stage bioreactor configuration. *Biotechnology and Bioengineering*, 1–10. https://doi.org/10.1002/bit.28507